The Oklahoma Mesonet's Skin Temperature Network

CHRISTOPHER A. FIEBRICH AND JANET E. MARTINEZ

Oklahoma Climatological Survey, Norman, Oklahoma

JERALD A. BROTZGE

Center for Analysis and Prediction of Storms, University of Oklahoma, Norman, Oklahoma

JEFFREY B. BASARA

Oklahoma Climatological Survey, Norman, Oklahoma

(Manuscript received 15 August 2002, in final form 13 March 2003)

ABSTRACT

In 1999, the Oklahoma Mesonet deployed infrared temperature (IRT) sensors at 89 of its environmental monitoring stations. A 3-yr dataset collected since that time provides a unique opportunity to analyze longer-term, continuous, mesoscale observations of skin temperature across a large area. Several limitations of the sensor have been identified and include 1) failure of the calibration equation during the cold season, 2) difficulty in keeping the sensor's lens clean at remote sites, and 3) limited representativeness of local conditions due to the sensor's narrow field of view. Despite these limitations, the Oklahoma Mesonet's skin temperature network provides a wealth of information that can be used to better understand many land–atmosphere interactions. Not only can the observations be used to estimate the partitioning of latent and sensible heat flux, they also provide beneficial ''ground truth'' estimates to validate remotely sensed estimates of skin temperature. This manuscript describes the IRT sensor, evaluates its performance, and provides analysis of time series data and observed spatial variability across Oklahoma.

1. Introduction

Land surface characteristics modulate the exchange of mass and energy between the land and atmosphere. While knowledge of the complex interactions between the surface and the atmosphere has increased in recent years, understanding nonlinear feedbacks within the biosphere–atmosphere system remains difficult. A limited number of observations have been available to better understand these feedbacks (Emanuel et al. 1995; Entekhabi et al. 1999). Many studies have relied upon datasets collected during intensive observing periods from short-lived field studies such as the First International Satellite Land Surface Climatology Project (ISLSCP) Experiment (FIFE) Project (Sellers et al. 1992), the Hydrological Atmospheric Pilot Experiment-Modelisation du Bilan Hydrique (HAPEX-MOBILHY; André et al. 1986), or the Southern Great Plains (SGP) experiments (Jackson et al. 1999).

Skin temperature (T_s), commonly defined as the temperature of the interface between the earth's surface and its atmosphere, is a critical variable to land–atmosphere interactions. For example, T_s is used by Monin–Obukhov similarity theory (1954) to estimate sensible heat flux (Kustas et al. 1989; Sugita and Brutsaert 1996; Cahill et al. 1997; Crago 1998; Lhomme et al. 2000; Voogt and Grimmond 2000). Furthermore, T_s is used to estimate latent heat flux (Crago 1998; Ibanez et al. 1999), air temperature and humidity (English 1999), bare soil evaporation (Katul and Parlange 1992), and leaf wetness (Deshpande et al. 1995).

Observed radiances via satellite observations provide spatial estimates of T_s from local to global scales. However, retrieval errors associated with satellite observations can lead to large errors in T_s estimates (Kerr et al. 1992; Xiang and Smith 1997). Unfortunately, ground observations used to validate the satellite-derived values of T_s are limited (Lakshmi and Susskind 2000). Another drawback of satellite-derived T_s is that the measurements cannot be made when cloud cover is present.

An alternative approach to satellite measurements of T_s has been designed and implemented by the Oklahoma Mesonet (Brock et al. 1995), an automated network of 115 meteorological stations evenly spaced across the state (Fig. 1). In 1999, infrared temperature (IRT) sen-

Corresponding author address: Christopher A. Fiebrich, Oklahoma Climatological Survey, 100 E. Boyd St., Suite 1210, Norman, OK 73019.
E-mail: chris@mesonet.org

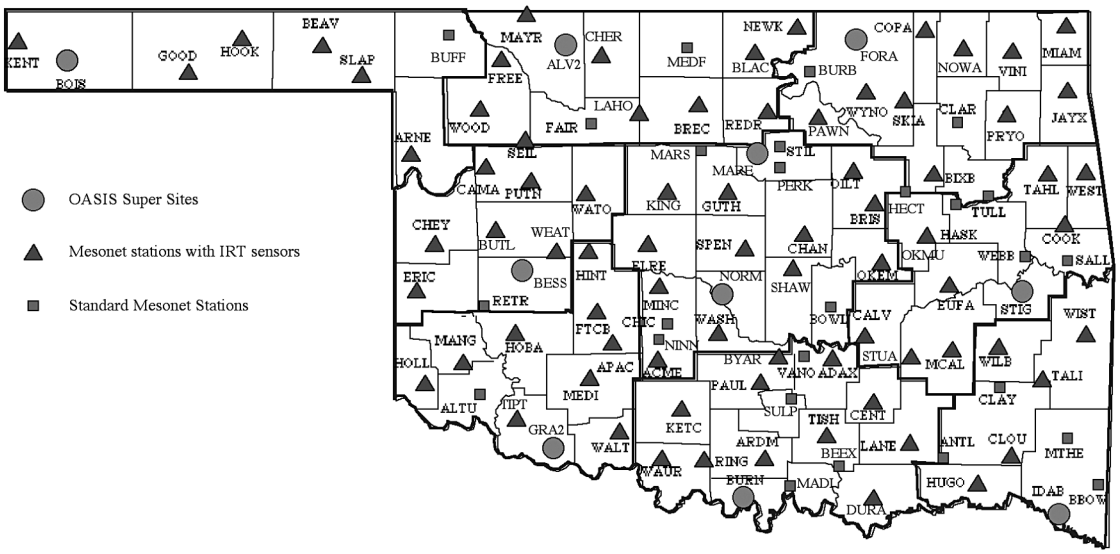

FIG. 1. Location of stations in the Oklahoma Mesonet.

sors were installed at 89 of the Mesonet sites. In addition, each Mesonet site measures solar radiation, air pressure, precipitation, wind speed and direction at 10 m, temperature and relative humidity at 1.5 m, and bare soil and sod temperatures at 10-cm depth. A majority of sites also measure wind speed at 2 and 9 m, temperature at 9 m, net radiation, soil moisture at 5-, 25-, 60-, and 75-cm depths, and soil temperatures at 5 and 30 cm. Furthermore, 10 sites that have IRT sensors installed are also designated as Oklahoma Atmospheric Surface-Layer Instrumentation System (OASIS) Super Sites (Fig. 1; Brotzge et al. 1999). In addition to the net radiation measurement, incoming and outgoing shortwave and longwave radiation are measured explicitly. The 10 Super Sites estimate sensible and latent heat flux (using an eddy covariance technique) and ground heat flux.

The objective of this manuscript is to provide an evaluation of 5-min-resolution field measurements collected using the 89 IRT sensors installed at Mesonet sites. The soil and atmospheric measurements collected by the Mesonet provide a unique opportunity to intercompare observations. This manuscript provides a description of the IRT sensor, an evaluation of its performance, and selected case studies that display the utility of the sensor and in situ observations of T_s.

2. Description of the IRT sensor

a. Sensor installation and calibration equation

The infrared thermometer used by the Oklahoma Mesonet is a precision thermocouple IRT manufactured by Apogee Instruments, Inc. (Bugbee et al. 1998). This sensor was chosen for use in the network because it is water resistant, designed for continuous outdoor use, and compatible with current Mesonet data acquisition systems. Sensor accuracy is approximately ± 0.2°C from 15° to 35°C and ± 0.3°C from 5° to 45°C. The sensor is installed at a height of 1.5 m and has a 3:1 field of view (i.e., a diameter circle field of view of 0.5 m).

As described by Planck's law, the intensity of energy emitted by a blackbody at a given wavelength is a function of the body temperature. With land surface temperatures spanning a 50°C range centered about 22°C (Fuchs 1990), the maximum terrestrial emission occurs at a wavelength near 10 μm. Infrared thermometers estimate skin temperature by measuring a specific waveband within the infrared range, typically 8–14 μm (Bugbee et al. 1998). The energy detected by the sensor is converted to a temperature using the Stefan–Boltzmann law and an assumed surface emissivity of 1.0. Slight underestimation is caused because the true emissivity of the land surface is less than 1.0. In addition, slight overestimation is caused by reflected longwave radiation from the target (Fuchs 1990).

The final (or calibrated) skin temperature (T_{sc}) is calculated as a function of the difference between the temperatures of the target (land–atmosphere interface) and sensor body. Errors can occur in measuring the sensor body temperature if the sensor is not isothermal, which then results in errors in T_{sc}. To minimize such errors, a large thermal mass surrounds the entire sensor to help maintain a more uniform and constant sensor body temperature during rapidly changing atmospheric conditions (Bugbee et al. 1998).

To account for errors introduced by the sensor body temperature, a correction provided by Apogee is applied to all observations. The correction is as follows:

$$T_{sc} = T_{target} - \frac{0.25}{P_{sb}}[(T_{target} - H_{sb})^2 - K_{sb}], \quad (1)$$

where T_{sc} is the calibrated skin temperature (°C), T_{target}

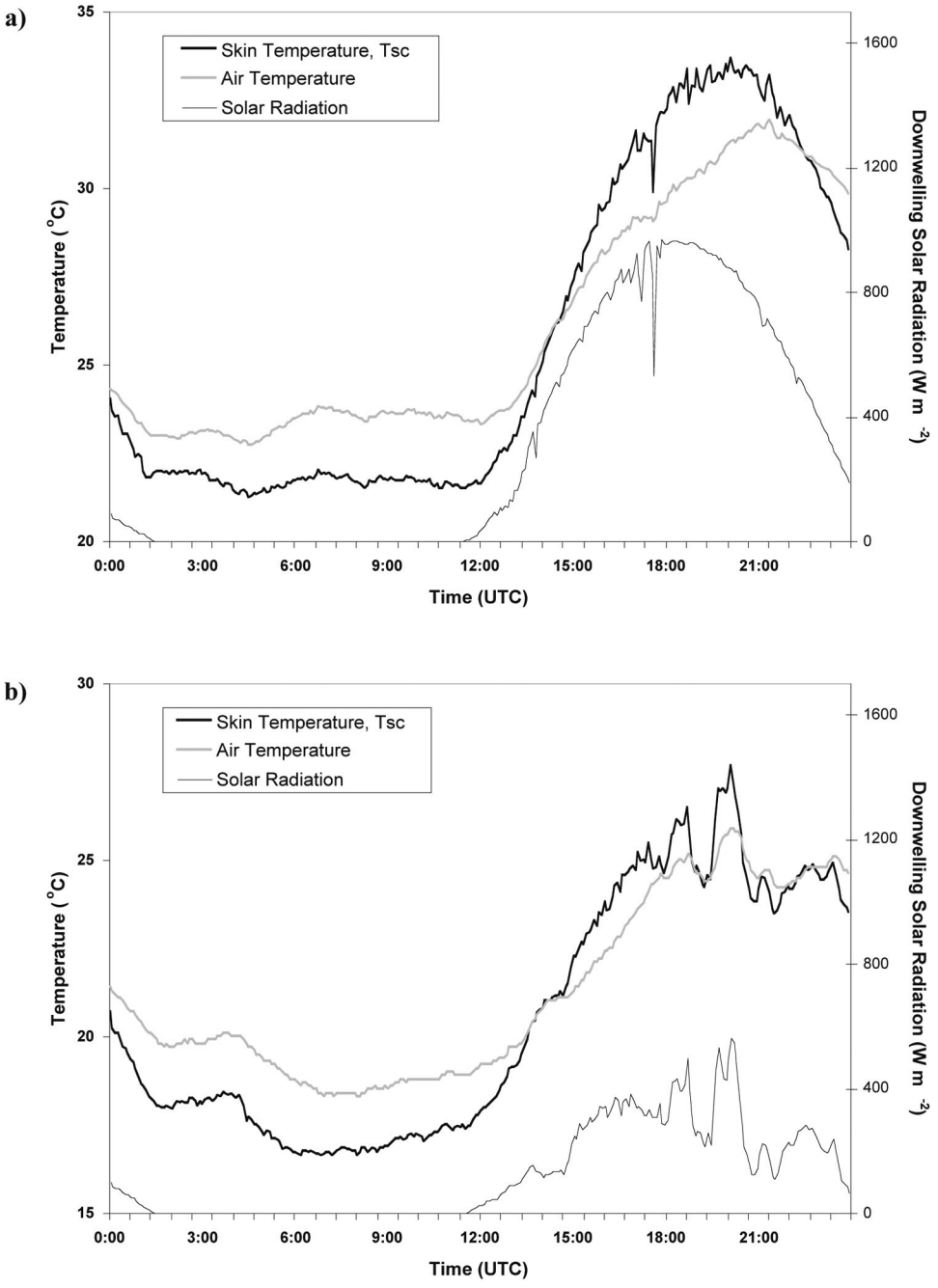

FIG. 2. Time series plot of the T_{sc} (°C), air temperature (°C), and downwelling solar radiation (W m^{-2}) at the Mesonet site near Marena, OK, on (a) 11 May and (b) 16 May 2000.

is the apparent target temperature (°C), and P_{sb}, H_{sb}, and K_{sb} are polynomials estimated as a function of the sensor body temperature (sb) as follows:

$$P_{sb} = 26.168 + 2.8291\text{sb} - 0.033\,29\text{sb}^2,$$

$$H_{sb} = 5.8075 - 0.080\,16\text{sb} + 0.008\,49\text{sb}^2,$$

$$K_{sb} = -85.943 + 11.740\text{sb} + 0.084\,77\text{sb}^2.$$

b. "Typical" data

A diurnal cycle of air temperature (measured at 1.5 m) and T_{sc} on 11 May 2000 at Marena, Oklahoma, is shown in Fig. 2a. Downwelling solar radiation, as measured by a LI-COR 200 pyranometer (Brock et al. 1995), is also shown. Both the air and skin temperatures decreased slightly near sunset at 0000 UTC (to convert to

local standard time for Oklahoma, subtract 6 h) and then remained nearly steady overnight. The T_{sc} remained slightly lower than the air temperature because of increased radiational cooling at the land surface. With sunrise at approximately 1200 UTC, both the air and skin temperature began a rapid increase. The T_{sc} increased quickly as a direct result of incoming solar radiation that heated the land surface. The time series shows that as downwelling solar radiation rapidly increased and decreased in response to intermittent cloudiness (specifically between 1600 and 1800 UTC), the T_{sc} also changed quickly. However, much smaller changes occurred in air temperature. This relationship illustrates the high sensitivity of T_{sc} to downwelling solar radiation.

The T_{sc} remained higher than air temperature for the majority of the daylight hours. While downwelling solar radiation peaked at solar noon (approximately 1800 UTC), the T_{sc} and air temperature peaked at about 1930 and 2130 UTC, respectively. These lag times denote the fact that downwelling shortwave radiation decreases in intensity after solar noon but still exceeds upwelling longwave radiation from the land surface for some time. This scenario yields an energy surplus for 2–4 h after solar noon and substantially contributes to a lag between the time of maximum solar heating and the time of maximum air and skin temperatures (Ahrens 2000). Skin temperature, being somewhat more sensitive to the decrease in downwelling solar radiation, begins its decrease prior to the decrease in air temperature.

In contrast, on a cloudy day at Marena (16 May 2000; Fig. 2b), the differences between the air and skin temperatures were reduced. The cloud cover decreased the skin temperature and created an isothermal layer near the surface. However, during intermittent increases in downwelling solar radiation, the skin temperature again demonstrated a rapid response.

3. Operation limitations

a. Limitation of the calibration equation

The Apogee IRT's calibrated range is from 5° to 45°C. Therefore, observations that fall outside of this temperature range may not be corrected properly by Eq. (1). In an effort to determine the utility of T_{sc} observations throughout a larger temperature range, 5-min observations of T_{sc} and outgoing longwave radiation [obtained from Kipp and Zonen CNR1 four-component radiometers (Brotzge and Duchon 2000)] were collected from three sites (Boise City in western Oklahoma, Marena in central Oklahoma, and Idabel in eastern Oklahoma) during April, August, and December 2000 (Fig. 3). Skin temperatures were estimated from the longwave (LW) radiation observations using the Stefan–Boltzmann law. Direct comparisons between the T_{sc} and CNR1 skin temperature estimates demonstrate the problems with using Eq. (1) during the cool season. The T_{sc} values tend to blow up when skin temperature estimates are below 0°C. Likewise, in this analysis, when skin temperatures are greater than 40°C, Eq. (1) overestimates skin temperatures by an average of 2.1°C. Despite this limitation, the cost of an Apogee IRT sensor (compared to that of a pyrgeometer) makes it an attractive sensor for a network with a limited budget.

b. Cleaning problem

Mesonet personnel have found that the surface lens on the Apogee IRT sensor can be difficult to keep clean at remote sites. When dust, spider webs, or other debris cover the lens, the sensor is unable to sense the land–atmosphere interface as its target. Instead, the obstruction on the lens becomes the target. These instances are often easy to detect in the observed data because the target and sensor body temperatures remain nearly equal. Such instances result in erroneous values of T_{sc}. For example, a 100+ day time series plot of the difference between the target and sensor body temperatures at the Chandler site is shown in Fig. 4; it represents the period 17 May–4 September 2001. From day 137 (17 May) through day 145 (25 May), the calculated difference exhibits a diurnal range between −5° and 10°C. Such a range is common because of radiational cooling and heating effects. However, from day 145 through day 235 (i.e., 17 May–23 August), when the viewing lens of the IRT was obstructed, the target and sensor body temperatures remained nearly equal. On day 236 (24 August), the IRT sensor lens was cleaned and the diurnal range varied from approximately −5° to 15°C.

This example illustrates the importance of keeping the IRT sensor clean while it is deployed in the field. An automated quality assurance algorithm that checks for differences between target and sensor body temperatures is an essential tool in identifying sensors with obstructed lenses. This technique, however, is only useful for IRT sensors that have separate outputs for sensor body and target temperatures. Although this problem is easily detected in the data, limited resources may prevent frequent technician visits to clean the sensors.

c. Footprint problem

Because all IRT sensors have a limited field of view (see section 2a), the observed T_{sc} values are sometimes not representative of larger-scale surface features. Vegetation properties can be significantly different inside the 10 m × 10 m Mesonet site plot when compared to vegetation conditions surrounding the plot. Only native vegetation is found within the site area; crops and grazed land often surround the site. This limitation cannot be overcome unless multiple IRT sensors are deployed over a broad area or the sensor is mounted hundreds of meters above the ground. An example of this limitation is well illustrated using observations across Oklahoma's winter wheat belt [a 150-km swath of winter wheat farms that

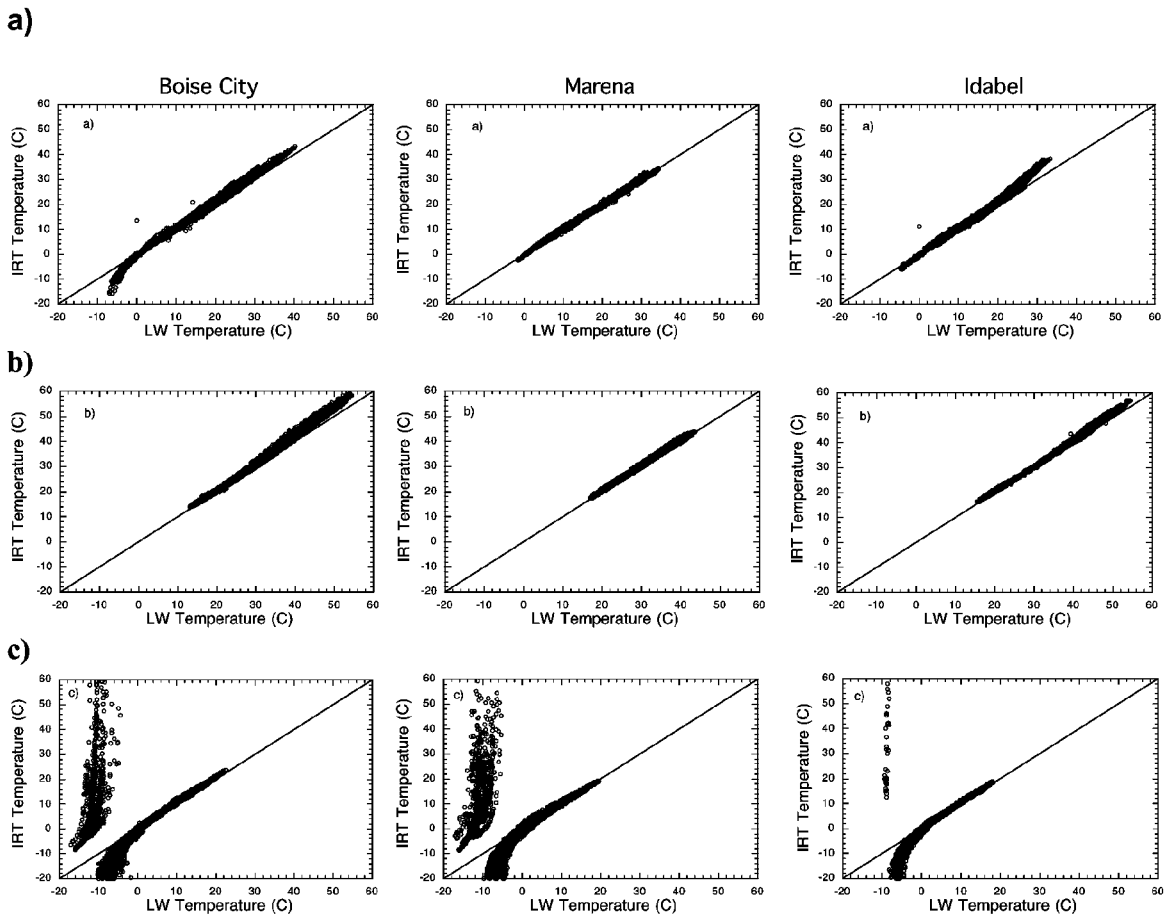

FIG. 3. Scatterplots of 5-min observations of skin temperature as measured by the IRT and as estimated from emitted longwave radiation. Data shown were collected during (a) Apr, (b) Aug, and (c) Dec 2000 at sites near (left) Boise City, (center) Marena, and (right) Idabel.

stretch from southwest to north-central Oklahoma (McPherson et al. 2004)].

The air temperature across Oklahoma at 1800 UTC 9 July 2001 is plotted in Fig. 5a. A warm anomaly

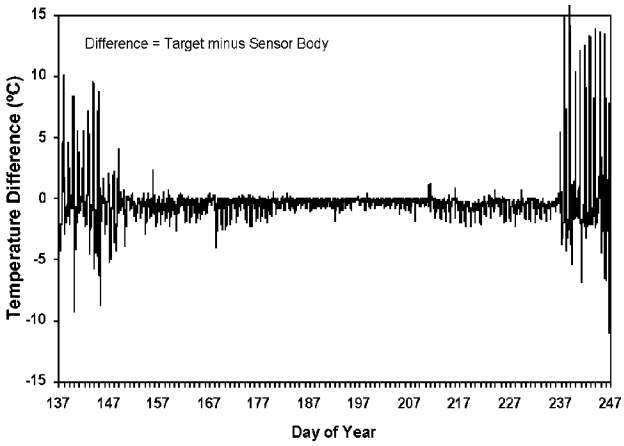

FIG. 4. Time series plot of the difference (°C) between the IRT target and sensor body temperatures for 17 May–4 Sep (days 137–247) 2001.

stretches across the winter wheat belt from southwestern to north-central Oklahoma. The region of harvested wheat fields is also apparent in a concurrent image of relative greenness (Fig. 5b). These relative greenness values were derived from 1-km-resolution data of the Normalized Difference Vegetative Index (NDVI; Burgan and Hartford 1993) from the Advanced Very High Resolution Radiometer (AVHRR) satellite. On this sunny day, the exposed soils across the harvested wheat belt created an increased partitioning of solar radiation to sensible heat flux. The result was a warm air temperature anomaly across parts of the Panhandle and western Oklahoma. It is impressive how close the warm air temperature anomaly matches the location of the lighter colored areas of relative greenness (which depict an absence of vegetation) in Fig. 5b. In contrast, the observed T_{sc} map (Fig. 5c) does not indicate the strong signal demonstrated by the air temperature (Fig. 5a). These contrasting results arise because the IRT sensor is located directly above the native vegetation within the site enclosure, whereas the air temperature sensor is impacted by a much larger upstream footprint that includes the harvested fields.

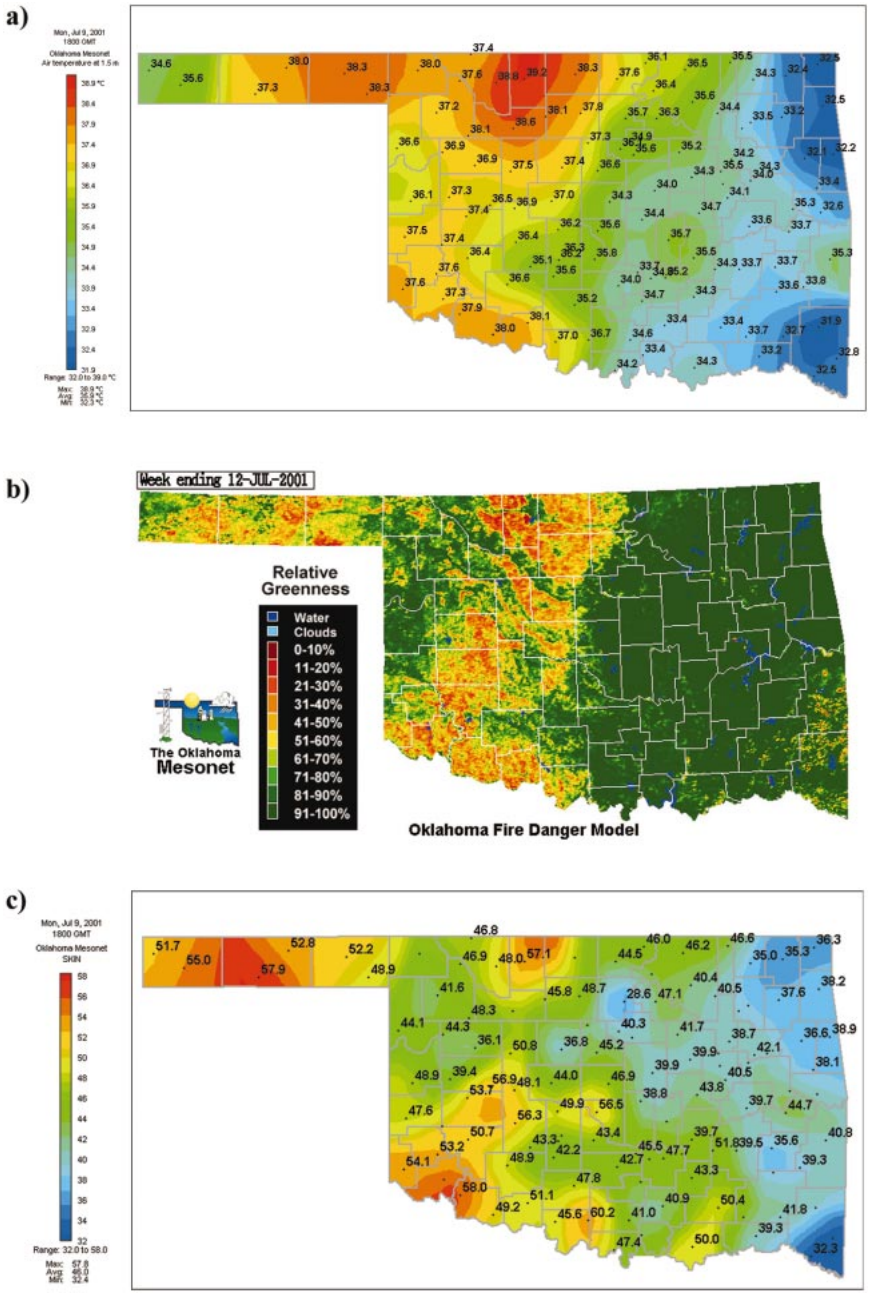

FIG. 5. (a) Mesonet station plot of the air temperature field (°C) across Oklahoma at 1800 UTC 9 Jul 2001. (b) Relative greenness values across Oklahoma derived from 1-km-resolution data of the NDVI on 12 Jul 2001 from the AVHRR satellite. (c) As in (a) except for the T_{sc} field (°C).

4. Observational spatial variability

Interesting mesoscale features are revealed by investigating patterns of T_{sc} across Oklahoma during clear-sky conditions. The observed T_{sc} values for 1500 UTC 12 July 2000 are shown in Fig. 6a. A large area of low T_{sc} values extended across the Panhandle into northwest Oklahoma. This cool anomaly corresponded well with the portion of the state that received rainfall the night before (Fig. 6b). In fact, the *relatively* high T_{sc} values at the Goodwell (GOOD), Hooker (HOOK), and Slapout (SLAP) stations in the Panhandle are attributed to the lack of rainfall at those three sites. Dry conditions in those areas increased the partitioning of available energy to sensible heat flux and produced mesoscale warm anomalies across the Panhandle. At sites that did receive rainfall, the additional moisture prevented the land surface from warming as rapidly (because of increased latent heat flux).

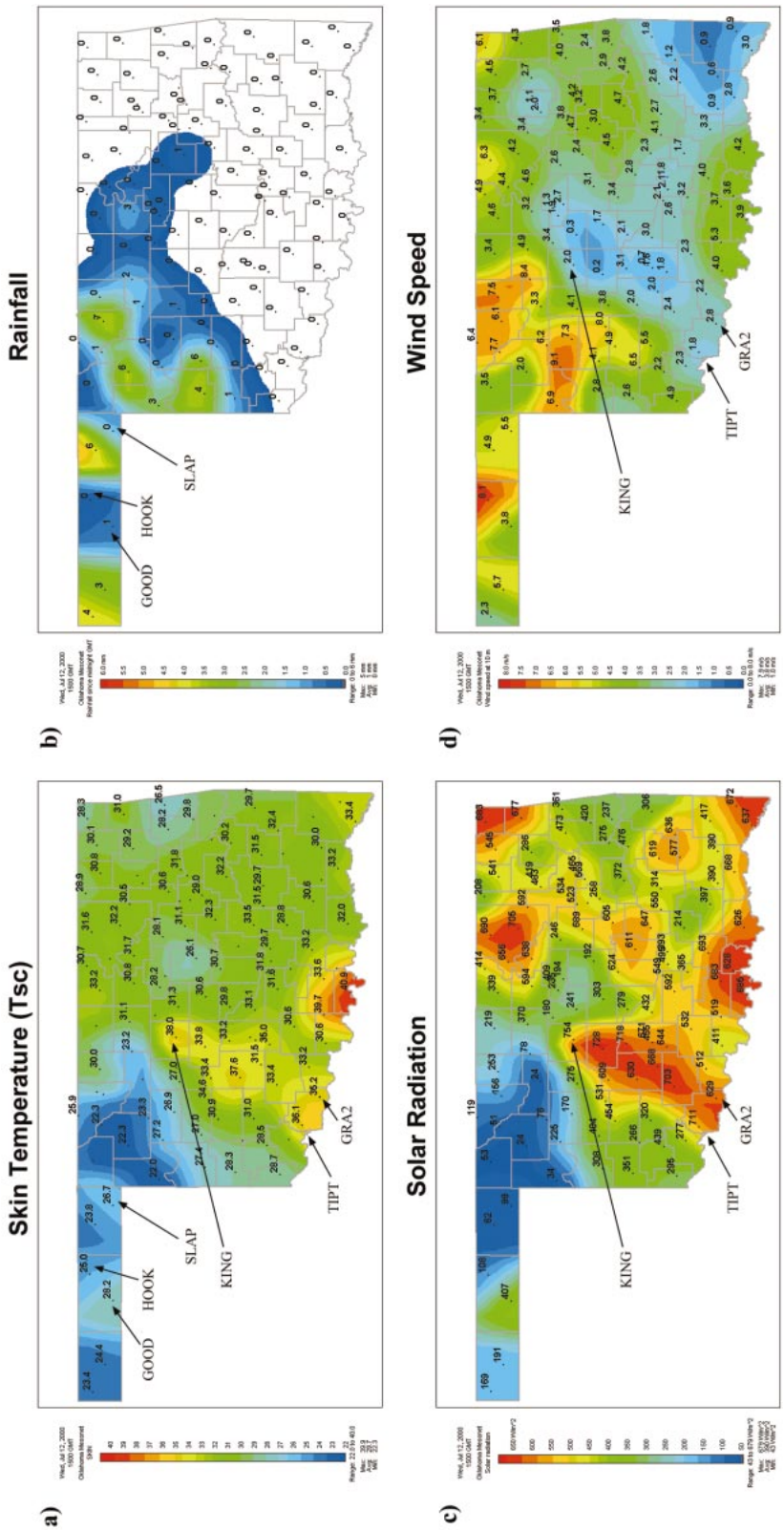

FIG. 6. (a) Mesonet station plot of the T_{sc} (°C) field across Oklahoma at 1500 UTC 12 Jul 2000. A large area of low T_{sc} values is apparent across the Panhandle and northwest Oklahoma. (b) As in (a) except for accumulated rainfall (mm) since 0000 UTC. (c) As in (a) except for solar radiation (W m^{-2}). (d) As in (a) except for wind speed (m s^{-1}).

The T_{sc} map (Fig. 6a) also revealed a lobe of high temperatures that extended from the Tipton (TIPT) and Grandfield (GRA2) stations in southwest Oklahoma northeast to the Kingfisher (KING) site. This area of high T_{sc} resulted from an increase in downwelling solar radiation (Fig. 6c). The incoming solar radiation heated the earth's surface and, with light winds (Fig. 6d), increased the T_{sc} in these areas. However, T_{sc} values do not reflect the numerous local maxima of solar radiation (Fig. 6c) throughout parts of eastern Oklahoma, because of stronger wind speeds in those locations (Fig. 6d).

5. Summary

The Oklahoma Mesonet installed IRT sensors at 89 sites across the state. Field evaluation demonstrated that obstructions on the lens of a sensor cause erroneous observations during continuous operational use outdoors. In addition, the calibration equation limited the use of the observations during the cold season. Lastly, care must be taken when extrapolating the observations spatially because of the sensor's narrow field of view.

Even with these limitations, the Oklahoma Mesonet's IRT network provides a unique opportunity to analyze long-term, continuous, mesoscale observations of skin temperature across a large area. Such observations may prove critical in understanding many land–atmosphere interactions. Not only can the observations be used to estimate the partitioning of latent and sensible heat flux, they also provide beneficial ''ground truth'' estimates to validate remotely sensed estimates of skin temperature.

Acknowledgments. The installation of the Oklahoma Mesonet's IRT network was made possible, in part, by NSF Grant 125-5645, EPSCoR 95 Grant NCC 5-171, and NOAA–University of Oklahoma Cooperative Agreement NA17RJ1227. Continued funding for maintenance of the network is provided by the taxpayers of the State of Oklahoma. The authors would like to thank Scott Richardson, James Kilby, David Grimsley, Leslie Cain, Kris Kesler, Ken Meyers, Bill Wyatt, and Thomas Smith for their professional assistance in maintaining the Oklahoma Mesonet. In addition, the authors would like to thank Ken Crawford, Director, and the staff of the Oklahoma Climatological Survey, whose innovative work makes such projects possible.

REFERENCES

André, J. C., J. P. Gourtorbe, and A. Perrier, 1986: HAPEX-MOBILHY: A hydrologic atmospheric experiment for the study of water budget and evaporation flux at the climatic scale. *Bull. Amer. Meteor. Soc.,* **67,** 138–144.

Ahrens, C. D., 2000: *Meteorology Today*. 6th ed. Brooks/Cole, 528 pp.

Brock, F. V., K. C. Crawford, R. L. Elliott, G. W. Cuperus, S. J. Stadler, H. L. Johnson, and M. D. Eilts, 1995: The Oklahoma Mesonet: A technical overview. *J. Atmos. Oceanic Technol.,* **12,** 5–19.

Brotzge, J. A., and C. E. Duchon, 2000: A field comparison among a domeless net radiometer, two four-component net radiometers, and a domed net radiometer. *J. Atmos. Oceanic Technol.,* **17,** 1569–1582.

——, S. J. Richardson, K. C. Crawford, T. W. Horst, F. V. Brock, K. S. Humes, Z. Sorbjan, and R. L. Elliott, 1999: The Oklahoma Atmospheric Surface-layer Instrumentation System (OASIS) Project. Preprints, *13th Conf. on Boundary-Layer Turbulence,* Dallas, TX, Amer. Meteor. Soc., 612–615.

Bugbee, B., M. Droter, O. Monje, and B. Tanner, 1998: Evaluation and modification of commercial infra-red transducers for leaf temperature measurement. *Adv. Space Res.,* **22,** 1425–1434.

Burgan, R. E., and R. A. Hartford, 1993: Monitoring vegetation greenness with satellite data. General Tech. Rep. INT-297, U.S. Department of Agriculture, Forest Service, Intermountain Research Station, Ogden, UT, 13 pp.

Cahill, A. T., M. B. Parlange, and J. D. Albertson, 1997: On the Brutsaert temperature roughness length model for sensible heat flux estimation. *Water Resour. Res.,* **33,** 2315–2324.

Crago, R. D., 1998: Radiometric and equivalent isothermal surface temperatures. *Water Resour. Res.,* **34,** 3017–3023.

Deshpande, R. Y., K. G. Hubbard, D. P. Coyne, J. R. Steadman, and A. M. Parkhurst, 1995: Estimating leaf wetness in dry bean canopies as a prerequisite to evaluating white mold disease. *Agron. J.,* **87,** 613–619.

Emmanuel, K., and Coauthors, 1995: Report of the first prospectus development team of the U.S. Weather Research Program to NOAA and the NSF. *Bull. Amer. Meteor. Soc.,* **76,** 1194–1208.

English, S. J., 1999: Estimation of temperature and humidity profile information from microwave radiances over different surface types. *J. Appl. Meteor.,* **38,** 1526–1541.

Entekhabi, D., and Coauthors, 1999: An agenda for land surface hydrology research and a call for the Second International Hydrological Decade. *Bull. Amer. Meteor. Soc.,* **80,** 2043–2058.

Fuchs, M., 1990: Canopy thermal infrared observations. *Remote Sens. Rev.,* **5,** 323–333.

Ibanez, M., P. J. Perez, J. I. Rosell, and F. Castellvi, 1999: Estimation of the latent heat flux over full canopy covers from the radiative temperature. *J. Appl. Meteor.,* **38,** 423–431.

Jackson, T. J., D. M. Le Vine, A. Y. Hsu, A. Oldak, P. J. Starks, C. T. Swift, J. D. Isham, and M. Haken, 1999: Soil moisture mapping at regional scales using microwave radiometry: The Southern Great Plains Hydrology Experiment. *IEEE Trans. Geosci. Remote Sens.,* **37,** 2136–2151.

Katul, G. G., and M. B. Parlange, 1992: Estimation of bare soil evaporation using skin temperature measurements. *J. Hydrol.,* **132,** 91–106.

Kerr, Y. H., J. P. Lagouarde, and J. Imbernon, 1992: Accurate land surface temperature retrieval from AVHRR data with use of an improved split window algorithm. *Remote Sens. Environ.,* **41,** 197–209.

Kustas, W. P., B. J. Choudhury, M. S. Moran, R. J. Reginato, R. D. Jackson, I. W. Gray, and H. L. Weaver, 1989: Determination of sensible heat flux using thermal infrared data. *Agric. For. Meteor.,* **44,** 197–216.

Lakshmi, V., and J. Susskind, 2000: Comparison of TOVS-derived land surface variables with ground observations. *J. Geophys. Res.,* **105,** 2179–2190.

Lhomme, J. P., A. Chehbouni, and B. Monteny, 2000: Sensible heat flux-radiometric surface temperature relationship over sparse vegetation: Parameterizing B^{-1}. *Bound.-Layer Meteor.,* **97,** 431–457.

McPherson, R. A., D. J. Stensrud, and K. C. Crawford, 2004: The impact of Oklahoma's winter wheat belt on the mesoscale environment. *Mon. Wea. Rev.,* in press.

Monin, A. S., and A. M. Obukhov, 1954: Basic laws of turbulent mixing in the ground layer of the atmosphere. *Tr. Geofiz. Inst. Akad. Nauk. SSSR,* **24,** 163–187.

Sellers, P. J., F. G. Hall, G. Asrar, D. E. Strebel, and R. E. Murphy, 1992: An overview of the First International Satellite Land Sur-

face Climatology Project (ISLSCP) Field Experiment (FIFE). *J. Geophys. Res.,* **97,** 18 345–18 373.

Sugita, M., and W. Brutsaert, 1996: Optimal measurement strategy for surface temperature to determine sensible heat flux from an isothermal vegetation. *Water Resour. Res.,* **32,** 2129–2134.

Voogt, J. A., and C. S. B. Grimmond, 2000: Modeling surface sensible heat flux using surface radiative temperatures in a simple urban area. *J. Appl. Meteor.,* **39,** 1679–1699.

Xiang, X., and E. A. Smith, 1997: Feasibility of simultaneous surface temperature-emissivity retrieval using SSM/I measurements from HAPEX-Sahel. *J. Hydrol.,* **188,** 330–360.